

See discussions, stats, and author profiles for this publication at: <https://www.researchgate.net/publication/234842476>

Charge Density Analysis of Ferulic Acid: Robustness of a Trifurcated C–H···O Hydrogen Bond

ARTICLE in CRYSTAL GROWTH & DESIGN · NOVEMBER 2012

Impact Factor: 4.89 · DOI: 10.1021/cg301211h

CITATIONS

18

READS

31

3 AUTHORS, INCLUDING:



Sajesh P Thomas

University of Western Australia

18 PUBLICATIONS 253 CITATIONS

[SEE PROFILE](#)



Pavan Mysore Srinivas

Indian Institute of Science

14 PUBLICATIONS 159 CITATIONS

[SEE PROFILE](#)

Charge Density Analysis of Ferulic Acid: Robustness of a Trifurcated C–H···O Hydrogen Bond

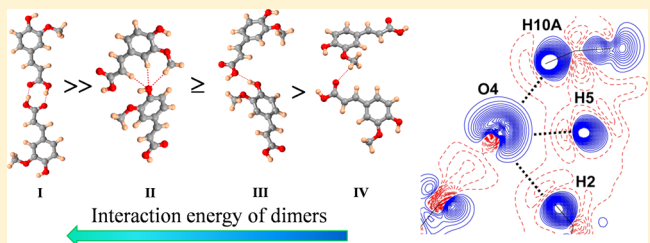
Published as part of the Crystal Growth & Design virtual special issue In Honor of Prof. G. R. Desiraju

Sajesh P. Thomas, Mysore S. Pavan, and Tayur N. Guru Row*

Solid State and Structural Chemistry Unit, Indian Institute of Science, Bangalore 560 012, India

Supporting Information

ABSTRACT: The topological features of a sporadic trifurcated C–H···O interaction region, where an oxygen atom acts as an acceptor of three weak hydrogen bonds, has been investigated by experimental and theoretical charge density analysis of ferulic acid. The interaction energy of the asymmetric molecular dimer formed by the trifurcated C–H···O motif, based on the multipolar model, is shown to be greater than the corresponding asymmetric O–H···O dimer in this crystal structure. Further, the hydrogen bond energies associated with these interaction motifs have been estimated from the local kinetic and potential energy densities at the bond critical points. The trends suggest that the interaction energy of the trifurcated C–H···O region is comparable to that of a single O–H···O hydrogen bond.



INTRODUCTION

The characteristics of a hydrogen bond are generally described in terms of its strength and directionality. Attempts to

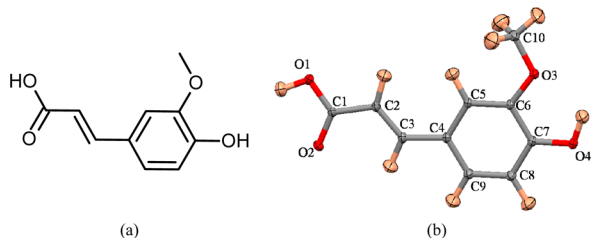


Figure 1. (a) Molecular structure of ferulic acid (b) ORTEP diagram (50% probability ellipsoids) with numbering scheme.

categorize hydrogen bonds based on these factors into strong and weak varieties have been made,^{1,2} though more detailed studies indicate a continuum of interaction regimes with no such clear borders between the weak and the strong.^{3–10} In this context, a nonconventional hydrogen bond like C–H···O interaction gains significance, particularly in terms of its role in forming supramolecular synthons.^{11–13} The nature and diversity of C–H···O hydrogen bonds, in fact, have direct implications in elucidating biological structures,^{14,15} protein–DNA recognition,¹⁶ drug–receptor interaction,^{14,17,18} transition state of catalytic processes^{19,20} and control of molecular conformations²¹ in general. The description and authentication of C–H···O interactions as a weak hydrogen bond and also as an essential crystal engineering element have been highlighted in several reviews and text books.^{2,22–24} On the basis of a large number of crystal structures, spectroscopic studies,^{25–27} and in

recent times using charge density approach²⁸ the underlying principles of C–H···O interactions have been established.^{29–38} The electrostatic component in the C–H···O hydrogen bond and its relevance in controlling crystal packing in the absence of other strong hydrogen bonds have been analyzed and the amount of electronic charge flow in the interaction region has been quantified.³⁹ However, multifurcated C–H···O interaction motifs, though observed,^{40,41} have not been subjected to rigorous evaluation in terms of their strength and directionality based on quantitative results obtained from charge density topology.

Bader's Atoms in Molecules (AIM)⁴² theory has been useful in deciphering quantum mechanical wave functions in terms of a real space observable, i.e., electron density, and its distribution in molecular space. Subtle and weak intermolecular interactions could be thus characterized in terms of the electron density topology. Early studies on theoretical charge density analysis in the gas phase showed that C–H···O interaction region satisfied certain topological criteria to be considered a hydrogen bond.⁴³ As multipole formalism offers a direct experimental means to map charge density of molecules in a crystalline environment, a variety of C–H···O hydrogen bonds have been characterized in terms of their topological parameters. The charge density topological parameters such as electron density, its derivatives and energy densities evaluated at the bond critical points of C–H···O hydrogen bonds are known to vary with respect to interaction geometry and environments.^{6,13,16,26,44–47} It has

Received: August 21, 2012

Revised: November 12, 2012

Published: November 15, 2012



also been pointed out that the flexibility associated with C–H···O hydrogen bonds (in terms of interaction distances and donor–acceptor angles) results in their ability to form multifurcated interaction motifs.⁴⁸ Hence, it is of importance to analyze the systematic trends in C–H···O hydrogen bonds present in multifurcated interaction motifs in order to establish the correlation between the geometry of interaction and the corresponding electron density topology.

In this article, we report the experimental and theoretical charge density features of ferulic acid, an organic phytochemical (Figure 1a).⁴⁹ Ferulic acid is known to be an *in vitro* antioxidant, reactive toward free radicals.⁵⁰ The end-to-end electron conjugation and resonance effects expected in this molecule have been examined based on charge density descriptors. Further, a rare trifurcated C–H···O interaction motif observed in the crystal structure of ferulic acid is characterized in terms interaction energies and topological parameters which allows for the comparison of C–H···O interactions with varying interaction geometry, keeping the acceptor oxygen atom the same.

EXPERIMENTAL SECTION

Crystallization. The commercially obtained sample of ferulic acid was crystallized by slow evaporation from acetonitrile. Good quality

Table 1. Crystallographic and Structure Refinement Details for Ferulic Acid

CCDC no.	894518	$(\sin \theta/\lambda)_{\max}$ (\AA^{-1})	1.08
molecular formula	$\text{C}_{10}\text{H}_{10}\text{O}_4$	reflns collected	118733
formula weight	194.18	unique reflns	9544
crystal system	monoclinic	completeness (%)	100
space group	$P2_1/n$	redundancy	12.4
<i>a</i> (\AA)	4.5887(1)	R_{int}	0.062
<i>b</i> (\AA)	16.7619(2)	Spherical atom refinement	
<i>c</i> (\AA)	11.7853(2)	R_1 (F)	0.0385
α ($^\circ$)	90	wR_2 (F^2)	0.1086
β ($^\circ$)	91.852(1)	goodness-of-fit	1.087
γ ($^\circ$)	90	$\Delta\rho_{\min/\max}$ ($e \text{\AA}^{-3}$)	-0.30, 0.72
<i>V</i> (\AA^3)	906.00(3)	Multipole refinement	
<i>Z</i>	4	reflns used [$I > 2\sigma(I)$]	7314
ρ_{calc} (g/cm^3)	1.424	N_{ref}/N_v	23
$F(000)$	408	R_1 (F^2)	0.0289
μ . (mm^{-1})	0.111	wR_2 (F^2)	0.0756
<i>T</i> (K)	100(2)	goodness-of-fit	1.1453
λ (\AA)	0.71073	$\Delta\rho_{\min/\max}$ ($e \text{\AA}^{-3}$)	-0.11, 0.14

single crystals were chosen using a polarizing microscope and affixed to a Hampton Research Cryoloop using Paratone-N oil.

Data Collection and Structure Refinement Details. A needle-shaped crystal of dimensions $0.42 \times 0.17 \times 0.15$ mm was cooled to 100 K with a liquid nitrogen stream using an Oxford Instruments Cryojet-HT nitrogen gas-stream cooling device. X-ray diffraction data were collected on an Oxford Xcalibur (Mova) diffractometer equipped with an Eos CCD detector using MoK α radiation ($\lambda = 0.71073 \text{\AA}$). The crystal-to-detector distance was fixed at 45 mm, and the scan width ($\Delta\omega$) was 1° per frame during the data collection. The data collection strategy was chosen in such a way to yield a high resolution X-ray data set ($(\sin \theta/\lambda)_{\max} = 1.08 \text{\AA}^{-1}$), with a high redundancy (~ 12) and completeness of 100% (Table S1, Supporting Information). Cell refinement, data integration and reduction were carried out using the program CrysAlisPro.⁵¹ Face indexing enabled an accurate numerical absorption correction. Sorting, scaling, and merging of the data sets were carried out using the program SORTAV.⁵² The crystal structure was solved by direct method using SHELXS97⁵³ and refined

based on the spherical-atom approximation (based on F^2) using SHELXL97⁵³ accessed by the WinGX package.⁵⁴ All hydrogen atoms were located from the difference Fourier map, and their position and isotropic thermal parameters were allowed to refine in the spherical atom model.

Multipole Modeling. The charge density modeling and multipolar aspherical atom refinements were performed based on the Hansen and Coppens multipole formalism⁵⁵ using XD2006.⁵⁶ The function, $\Sigma w [F_o|^2 - K|F_c|^2]^2$ was minimized for all reflections with $I > 2\sigma(I)$. Weights (w) were taken as $1/\sigma^2 (F_o^2)$ and the convergence criterion of the refinement was set to a maximal shift/esd $< 10^{-10}$. Su-Coppens-Macchi wave functions⁵⁷ were used for the core and valence scattering factors of all the atoms. The scale factor was refined against the whole resolution range of diffraction data in the first refinement step. The scatter plots showing the variation of F_{obs} with F_{cal} is indicative of the good quality of the data set after scaling (see Supporting Information, Figures S1 and S2). The positional and anisotropic displacement parameters of the non-hydrogen atoms were refined using reflection data with $\sin \theta/\lambda > 0.7 \text{\AA}^{-1}$. In the next step of refinement, the position and displacement parameters of the non-hydrogen atoms were fixed to the refined values. The procedure described by Hoser et al.⁵⁸ was employed to locate the hydrogen atom positions via a mixed refinement (using reflections $\sin \theta/\lambda < 0.7 \text{\AA}^{-1}$). Further, the X–H bond lengths were constrained to neutron values⁵⁹ followed by the estimation of anisotropic thermal parameters using the SHADE2 analysis.^{60,61}

ADP values of H-atoms obtained from SHADE2 analysis were kept fixed during the subsequent multipole refinements. Further, scale, positional and anisotropic displacement parameters, P_{val} , P_{lm} , κ , and κ' on non-hydrogen atoms were refined in a stepwise manner, until the convergence criterion was reached. Separate κ and κ' were used to define different non-H atom type based chemical environments with a common κ for all H-atoms. The multipole expansion was carried out up to octupole level ($l = 3$) for all non-hydrogen atoms. Chemical constraints were initially introduced for the multipole refinements of non-H atoms and released at a later stage of refinement owing to the improvements observed in the model. For H atoms, only monopole, bond directed dipole (d_z) and quadrupole (q_{3z^2-1}) components were refined during the refinement.

The quantitative analysis of the electron density topology and related properties was performed using the XDPROP and TOPXD⁶² modules of the XD software suite.⁵⁶ Crystallographic refinement details of both spherical and multipolar model are summarized in Table 1.

Computational Details. Positional parameters obtained from the experimental charge density model have been used for a single point periodic quantum mechanical calculations at the B3LYP/6-31G** level^{63,64} and TZVP level^{65,66} using the CRYSTAL09 package.⁶⁷ The shrinking factors (IS1, IS2, and IS3) and the reciprocal lattice vectors were set to 4 (with 30 k-points in irreducible Brillouin zone). The bielectronic Coulomb and exchange series values for the truncation parameter were set as ITOL1–ITOL4 = 8, and ITOL5 = 17, respectively, for the calculations. 0.7 hartree/cycle was set as the value for level shifter. An SCF convergence limit of the order of 10^{-6} Hartree was used.

In the static model, atomic thermal displacement parameters for all atoms were set to zero. Structure factors were calculated for a resolution of 1.08\AA^{-1} , which were used for the theoretical multipolar model. Refinements and analysis of the theoretical charge density model were performed using the XD software package following the same methodology used for the experimental charge density modeling.

RESULTS AND DISCUSSION

Crystal Structure. The crystal structure of ferulic acid was redetermined in this study and is akin to that reported in the literature.⁶⁸ The carboxylic acid dimer synthon governs the crystal packing with strong O–H···O hydrogen bonds. These synthons are interconnected via O–H_(phenolic)···O_(carboxylic) hydrogen bonds resulting in a sheet-like arrangement parallel

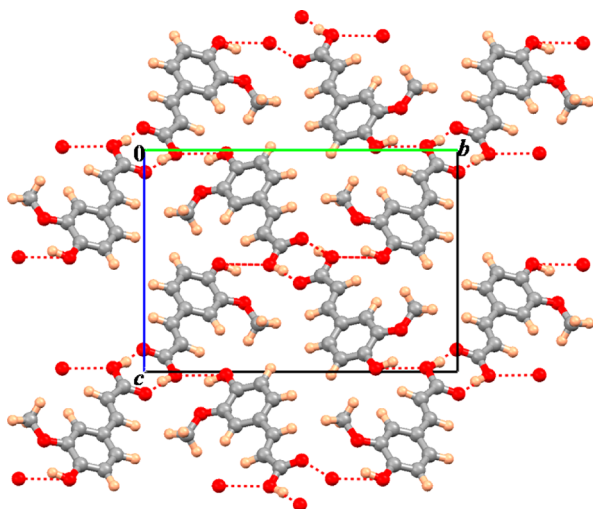


Figure 2. Crystal packing viewed down the a -axis, showing two different types of $\text{O}-\text{H}\cdots\text{O}$ hydrogen bonds.

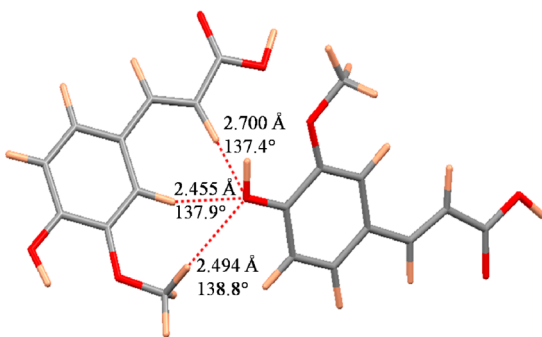


Figure 3. Intermolecular trifurcated $\text{C}-\text{H}\cdots\text{O}$ interaction motif in ferulic acid.

to (103) planes (Figure 2). These sheets are further packed by $\pi\cdots\pi$ interactions involving the phenyl ring and the $\text{C}=\text{C}$ region assisted by a variety of $\text{C}-\text{H}\cdots\text{O}$ interactions. Interestingly, the structure exhibits a trifurcated $\text{C}-\text{H}\cdots\text{O}$ interaction motif with the phenolic oxygen atom acting as a hydrogen bond acceptor from three different $\text{C}-\text{H}$ donors (Figure 3). These interactions involve a methyl $\text{C}-\text{H}$ (2.494 \AA , 138.8°), an aromatic $\text{C}-\text{H}$ (2.455 \AA , 137.9°), and an alkenic $\text{C}-\text{H}$ (2.700 \AA , 137.4°) acting as hydrogen bond donors, from a symmetry generated molecule ($1/2 + x$, $1/2 - y$, $-1/2 + z$) (Figure 3). This characteristic interaction motif with varying $\text{C}-\text{H}\cdots\text{O}$ interaction geometries provides us with an excellent prototype case to study a multifurcated $\text{C}-\text{H}\cdots\text{O}$ hydrogen bond.

A Cambridge Structural Database (CSD) analysis carried out to search for the trifurcated $\text{C}-\text{H}\cdots\text{O}$ interaction motif in molecular crystals resulted in 466 hits with phenolic oxygen atom as the acceptor (CSD v5.33, Feb 2012). However, crystal structures with this motif occurring between two molecules (as given in Figure 3) resulting in a dimeric assembly are found to be rare (25 hits in CSD, see Table S2 in Supporting Information for the details). While 14 hits out of these belong to single component structures, a remaining 11 hits are multicomponent structures (3 of them have the interaction motif occurring between different molecular components). Among these 25 structures, one forms a pentafurcated $\text{C}-\text{H}\cdots\text{O}$ interaction, while three others form tetrafurcated motifs.

It may be argued that the formation of multifurcated $\text{C}-\text{H}\cdots\text{O}$ interactions is significantly influenced by the number of $\text{C}-\text{H}$ groups on the molecule suitably oriented to form a dimeric assembly. However, the question whether they lead to a stable supramolecular synthon needs to be addressed via specific crystal engineering experiments.

Multipole Modeling. The electron density topological features of all the intermolecular interactions have been explored using experimental and theoretical charge density analysis. The final choice of the multipole model was made after a careful evaluation of several refinement strategies based on the final residual density features, nature of fractal dimension plot⁶⁹ and the resulting R-factors. The Hirshfeld rigid bond test⁷⁰ was applied to all covalent bonds involving non-hydrogen atoms to evaluate the quality of multipole modeling after the final cycle of refinement. The $\text{O}3-\text{C}10$ single bond is found to have the largest difference of mean-square displacement amplitude (DMSDA) value of 1×10^{-3} . The result of multipole refinements (with $I > 2\sigma(I)$) shows residual electron density peaks of $-0.11 \text{ e}/\text{\AA}^3$ and $0.14 \text{ e}/\text{\AA}^3$ with an RMS value of $0.05 \text{ e}/\text{\AA}^3$ for minimum and maximum values respectively. The corresponding values in theoretical charge density model vary from $-0.06 \text{ e}/\text{\AA}^3$ and $0.06 \text{ e}/\text{\AA}^3$ respectively with an RMS value of $0.02 \text{ e}/\text{\AA}^3$. The dipole moment derived from the experimental model (12.1 D) does not compare well with the values obtained from the theoretical models (6.2 D for TVZP model and 5.4 D for 6-31G**). However, this is not unusual for molecular crystals,⁷¹ especially when the experimental X–H bond lengths were constrained to standard neutron values.

The fractal dimension plot is symmetric in nature and parabolic in shape (see Supporting Information, Figures S3–S5). It is to be noted that fractal dimension plot provides the overall distribution of residual electron density in the unit cell and the associated net charge neutrality as derived from the multipole modeling.

Charge Density Topological Features. Static deformation density maps are clearly indicative of the aspherical nature of electron density distribution predominantly around oxygen atoms (Figure 4). Atom O2 represents classical “ sp^2 hybridized” lone pair characteristics, whereas O1, O3, and O4 have two lone pairs oriented in a way depicting a typical “ sp^3 hybridized” Lewis representation. The static deformation density and Laplacian maps from both experimental and theoretical models show that the covalent bond regions (except X–H bonds) have nearly similar charge density features suggesting a conjugation effect. The charge density topological properties for all the covalent bonds are listed in Tables S3 and S4 (Supporting Information). The values of electron density at the bond critical point (BCP), $\rho(r_b)$ and its curvature in space (given by Laplacian), $\nabla^2\rho(r_b)$ of various covalent bonds provide further evidence of conjugation. Another important topological descriptor, the bond ellipticity parameter (ϵ), is a representation of the cross sectional features of any bond at BCP. In the structure of ferulic acid all covalent bonds (except X–H bonds) show similar ellipticity values, thus indicating the conjugation effect (Tables S3 and S4) in the entire molecular space.

The net atomic charge on each atom is calculated as the difference between the valence population parameter (P_{val}) and the number of valence electrons in the free neutral atom (N_{val}). P_{val} and N_{val} are obtained from the charge density model (given in Supporting Information, Table S3). A more realistic description of atomic partial charges obtained via quadrature

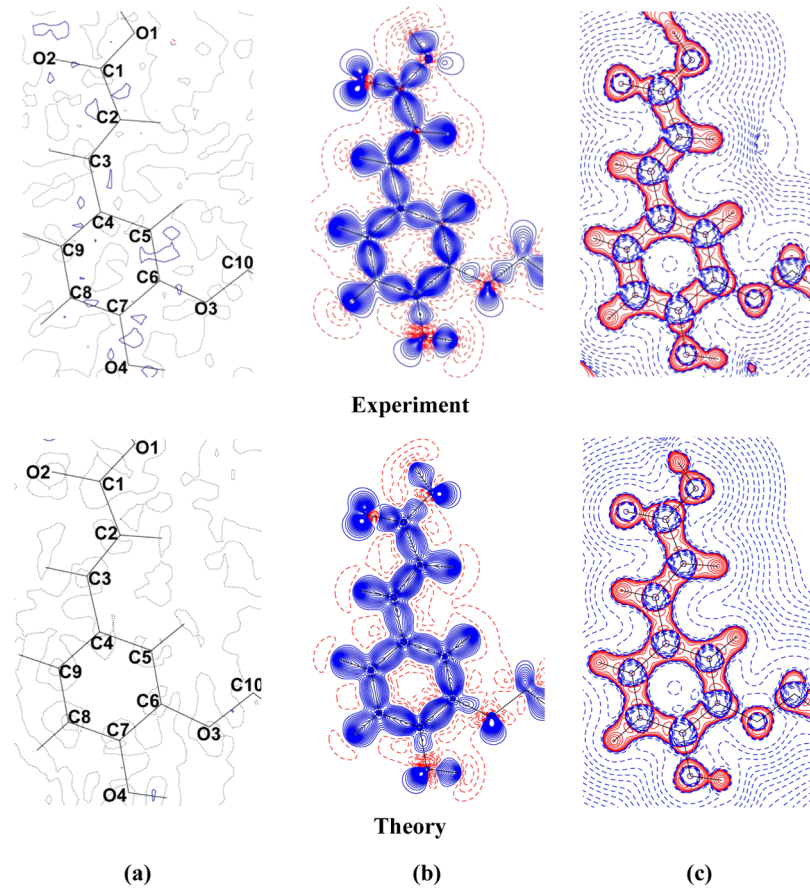


Figure 4. (a) Residual, (b) deformation, and (c) Laplacian of density maps generated from the experimental and theoretical (CRYSTAL09 B3LYP/TZVP periodic calculations) multipolar models of ferulic acid. Blue (solid lines), red (broken lines), and black (dotted lines) colors represent positive, negative, and zero contours, respectively. Contours are drawn at the intervals of $\pm 0.05 \text{ e } \text{\AA}^{-3}$.

Table 2. Stockholders Charge Obtained from the Experimental and Theoretical Charge Density Models

atom	experimental	theoretical		atom	experimental	theoretical	
		6-31G**	TZVP			6-31G**	TZVP
O(1)	-0.15	-0.23	-0.21	C(9)	-0.11	-0.01	-0.05
O(2)	-0.24	-0.28	-0.22	C(10)	-0.08	-0.08	-0.07
O(3)	-0.21	-0.19	-0.16	H(1)	0.29	0.23	0.23
O(4)	-0.27	-0.26	-0.22	H(2)	0.19	0.10	0.10
C(1)	0.18	0.16	0.15	H(3)	0.12	0.08	0.08
C(2)	-0.03	-0.06	-0.08	H(5)	0.14	0.08	0.08
C(3)	-0.05	0.02	-0.01	H(8)	0.07	0.05	0.05
C(4)	-0.04	0.00	-0.03	H(9)	0.09	0.08	0.08
C(5)	-0.01	-0.04	-0.04	H(10A)	0.09	0.06	0.06
C(6)	-0.04	0.01	0.01	H(10B)	0.06	0.06	0.07
C(7)	-0.08	0.05	0.02	H(10C)	0.07	0.05	0.06
C(8)	-0.16	-0.05	-0.08	H(4O)	0.22	0.18	0.18

integration on each atom (stockholders charge) is given in Table 2. Similarly, Atoms In Molecules (AIM) theory offers the possibility of estimating the net charges via integration over the individual atomic basins, resulting in AIM charges (see Table 3).

The trends in the stockholders charge and the AIM charges correlate with the corresponding values of the theoretical models (Figure 5). Thus, the theoretical models can serve as the validating tools to verify the trends in properties such as electrostatic and net interaction energies of the various

molecular dimers in this structure (discussed later in this study).

A topological analysis of the electron density located several (3,−1) bond critical points corresponding to the O—H···O and C—H···O interactions. The topological descriptors such as R_{ij} (interaction distance), $\rho(r_b)$, $\nabla^2\rho(r_b)$ and ε , evaluated at the BCPs of these interaction regions are listed in Table 4. As expected, the value of electron density at the BCP, $\rho(r_b)$, is highest for the O—H···O hydrogen bond in the carboxylic acid dimer synthon, followed by the corresponding values of $\rho(r_b)$ for O—H_(phenolic)···O_(carboxylic) and C—H···O hydrogen bonds

Table 3. AIM Charges, q (Ω) Obtained from the Experimental and Theoretical (B3LYP/TVZP) Charge Density Models

atom	experimental q (Ω)	theoretical q (Ω)	atom	experimental q (Ω)	theoretical q (Ω)
O(1)	-1.05	-0.95	C(9)	-0.01	-0.05
O(2)	-0.89	-0.78	C(10)	0.52	0.19
O(3)	-1.07	-0.86	H(1)	0.74	0.55
O(4)	-1.14	-0.93	H(2)	0.14	0.26
C(1)	1.17	1.07	H(3)	0.17	0.11
C(2)	0.15	-0.03	H(5)	0.16	0.10
C(3)	-0.02	-0.03	H(8)	-0.04	0.04
C(4)	-0.1	-0.01	H(9)	-0.02	0.07
C(5)	0.09	-0.02	H(10A)	0.03	0.12
C(6)	0.41	0.33	H(10B)	0.01	0.08
C(7)	0.27	0.35	H(10C)	-0.02	0.12
C(8)	0.00	-0.02	H(4O)	0.62	0.53

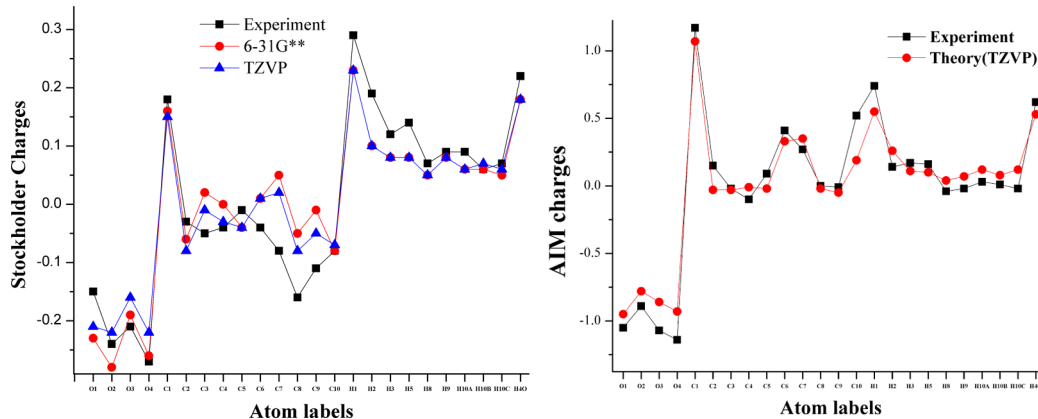


Figure 5. The correlations observed for stockholders charge and AIM charges obtained from the experimental and theoretical charge density models.

Table 4. Comparisons of the *bcp* Properties for Intermolecular Interactions Obtained from Experimental Charge Density Model and the Corresponding Theoretical Models^a

interaction	R_{ij} (\AA)	d_1 (\AA)	d_2 (\AA)	ρ ($e \text{ \AA}^{-3}$)	$\nabla^2\rho$ ($e \text{ \AA}^{-5}$)	ϵ	G ($\text{kJ mol}^{-1}\text{bohr}^{-3}$)	V ($\text{kJ mol}^{-1}\text{bohr}^{-3}$)
O1-H1…O2 ^a	1.6199	1.1024	0.5175	0.39	1.0	0.01	83.51	-138.72
6-31G**	1.6194	1.0846	0.5348	0.36	2.6	0.01	104.01	-138.41
TZVP	1.6191	1.0819	0.5372	0.35	3.1	0.00	111.84	-138.00
O4-H4O…O1 ^b	1.9773	1.2752	0.7022	0.13	1.7	0.23	41.21	-36.61
6-31G**	1.9784	1.2600	0.7184	0.14	1.9	0.21	44.98	-39.51
TZVP	1.9747	1.2607	0.7141	0.12	2.2	0.20	50.28	-39.56
C10-H10c…O2 ^c	2.5184	1.4510	1.0674	0.05	1.0	0.44	19.57	-12.75
6-31G**	2.4971	1.4456	1.0515	0.05	0.9	0.61	19.29	-12.82
TZVP	2.5022	1.4379	1.0643	0.05	0.9	0.46	19.08	-12.60
C2-H2…O4 ^d	2.7680	1.7444	1.0237	0.02	0.3	0.99	6.33	-3.97
6-31G**	2.7129	1.6128	1.1002	0.03	0.5	0.49	9.68	-6.43
TZVP	2.7032	1.6076	1.0956	0.03	0.5	0.51	10.05	-6.38
C5-H5…O4 ^d	2.4898	1.4893	1.0005	0.04	0.9	0.11	17.44	-11.19
6-31G**	2.4552	1.4580	0.9972	0.05	0.9	0.28	17.98	-12.49
TZVP	2.4564	1.4551	1.0012	0.05	0.9	0.21	18.07	-12.21
C10-H10A…O4 ^d	2.4946	1.4933	1.0013	0.05	0.8	0.46	16.80	-11.16
6-31G**	2.4945	1.4699	1.0247	0.05	0.8	0.29	16.32	-11.12
TZVP	2.4951	1.4690	1.0261	0.05	0.8	0.26	16.33	-10.93

^aSymmetry operations (a) $-x, -y, -z$; (b) $1/2 - x, -1/2 + y, 1/2 - z$; (c) $1/2 - x, -1/2 + y, 1/2 - z$; (d) $1/2 + x, 1/2 - y, 1/2 + z$.

(Table 3). The values of $\rho(r_b)$ and $\nabla^2\rho(r_b)$ and their trends correlate well with those of corresponding theoretical models (see Supporting Information Figure S6). This correlation is a crucial criterion to analyze and validate the relative strengths of stabilizing interactions in the crystal structure. Both these values decide the magnitude of interaction energy associated with individual intermolecular interactions.⁵ A notable deviation in

the values of $\nabla^2\rho(r_b)$ between experiment and theory is observed in the case of O1-H1…O2 hydrogen bond in the carboxylic acid dimer region. This is also apparent in a comparison of the Laplacian map obtained from experiment with that from theory (Figure 4c). This deviation can be attributed to the partial positional disorder usually associated with protons in the carboxylic acid dimer region. It is to be

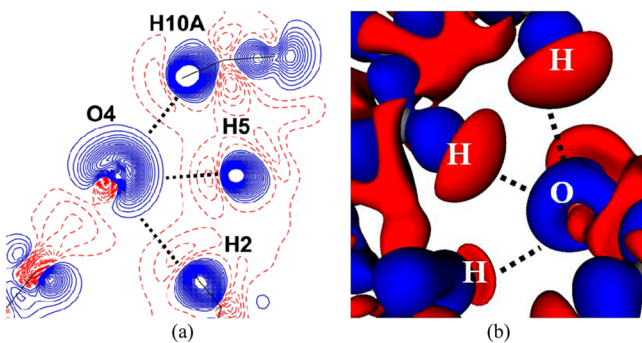


Figure 6. 2D and 3D static deformation density map generated from the experimental model showing the trifurcated C–H…O hydrogen bond region.

noted that the experimental model has the proton position (of H1) fixed from the neutron value of 1.018 Å, while actual proton positions can be statistically dispersed around that. The theoretical structure factors, calculated for fixed O1–H1 bond lengths, do not take account of this positional disorder. Further, the values of kinetic energy density (G_{cp}) and potential energy $V(r)$ density and their ratios exhibit trends anticipated for O–H…O and C–H…O hydrogen bonds.

It is of interest to note the trend in the electron density values at the critical points, $\rho(r_b)$, of the trifurcated C–H…O hydrogen bond region. The magnitude of $\rho(r_b)$ which generally correlates with the strength of the corresponding hydrogen bond follows the order C10–H10A_(methyl)…O4 > C5–H5_(aromatic)…O4 > C2–H2_(alkenyl)…O4. Interestingly, the relatively less acidic C–H_(methyl) proton forms a stronger hydrogen bond among the three. This seemingly counterintuitive order can be understood in terms of the geometry of interaction; While the hydrogen bond angle θ in each case is similar ($\theta = \angle C10–H10A–O4 = 138.8^\circ$, $\angle C5–H5–O4 = 137.9^\circ$, $\angle C2–H2–O4 = 137.4^\circ$), the value of the ϕ angle⁴⁸ is different ($\phi = \angle C7–O4–H5_{(aromatic)} = 120.5^\circ$, $\angle C7–O4–H10A_{(methyl)} = 123.0^\circ$, $\angle C7–O4–H2_{(alkenyl)} = 89.2^\circ$ respectively). Thus, based on the geometrical criteria alone the hydrogen bond C2–H2…O4 falls in an unfavorable region. In fact the electron density value is also indicative of this feature with a lower electron density at the BCP for this contact ($\rho(r_b) = 0.02$). However, the electron density value is significant enough to qualify C2–H2…O4 as a weak hydrogen bond from the charge density analysis point of view.

The significance of lone pair directionality manifested as the ϕ angle dependence of hydrogen bond strength is also apparent from the features in 2D deformation map (Figure 6a). The 3D

deformation density map of the trifurcated C–H…O interaction region clearly shows the charge concentrated region near oxygen atom and the charge depletion regions corresponding to C–H protons (Figure 6b). The blue region at the oxygen atom in the map represents the aspherical electron density distribution of the lone pairs, which are directed toward the red electropositive regions of the hydrogen atoms.

Figure 7 shows the electrostatic potential mapped on electron density isosurfaces around an isolated molecule extracted from the crystal lattice using XD2006 and visualized using the package MoleCoolQt.⁷² The isosurface values are drawn at 0.5 e Å⁻³ and the areas colored blue, red, and green represent electropositive, electronegative and neutral regions, respectively. The oxygen atoms belong to red regions, and the carbon atoms are in the blue region representing their partial charge character. The positive polarization on hydrogen atoms is apparent as blue regions on the ESP isosurface. It is interesting to note that the three hydrogen atoms H2, H5, H10A and the acceptor oxygen atom O4 involved in the trifurcated C–H…O interaction region are seen as the intense blue and red regions, respectively, on the isosurface.

Analysis of Interaction Energy. Electrostatic interaction energies of various molecular dimers are calculated using Exact Potential and Multipole Moments (EPMM)⁷³ algorithm in XD2006. In this algorithm, quadrature integration of the Exact Coulomb potential is used to evaluate short-range interatomic interactions, while long-range interatomic interactions are evaluated via multipole expansion in atomic moments. The net interaction energy of the dimers are further estimated by appending the electrostatic energy terms with exchange-repulsion and the dispersion terms calculated using Williams-Cox potential.⁷⁴ Energy values of the following molecular dimers are evaluated: (a) carboxylic acid dimer (I) (b) dimer formed by the trifurcated C–H…O interaction (II), and (c) dimer formed by O–H_(phenolic)…O_(carboxylic) hydrogen bond (III), (d) dimer formed by C–H_(methyl)…O_(carboxylic) hydrogen bond (IV) (Figure 8). The energy values arrange in the following order: I > II > III > IV. Remarkably, the trifurcated C–H…O dimer (II) is more stable than the corresponding asymmetric O–H…O dimer (III)! The fact that three C–H…O hydrogen bonds collectively surmount a classical O–H…O hydrogen bond is reminiscent of the Gulliver–Lilliputians analogy⁷⁵ of the weak intermolecular forces acting in a cooperative fashion.

The calculation of interaction energies have been also evaluated using the EML method,^{44,50} which utilizes solely the topological parameters such as ρ and $\nabla^2\rho$ at the BCPs. The

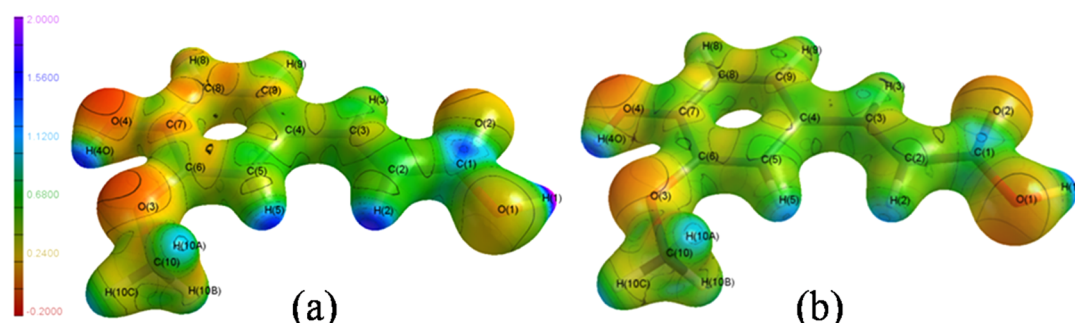


Figure 7. Electrostatic potential isosurface maps obtained from (a) experimental and (b) theoretical charge density methods, drawn at an isosurface value of 0.5 e Å⁻³. Blue and red colors represent electropositive and electronegative regions, respectively.

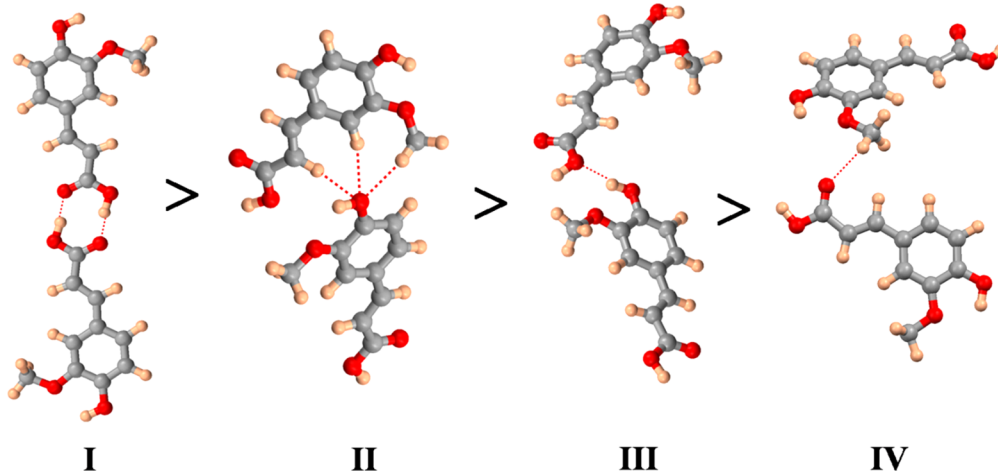


Figure 8. Molecular dimers formed by (I) O–H···O_(carboxylic) hydrogen bonds, (II) trifurcated C–H···O_(phenolic) hydrogen bond (III) O–H_(phenolic)···O_(carboxylic) hydrogen bond (IV) C–H_(methyl)···O_(carboxylic) hydrogen bond, in their decreasing order of interaction energies.

Table 5. Interaction Energies Obtained for the Molecular Dimers (EPMM) and the Associated Hydrogen Bond Energies (E_{HB}) Calculated from $\rho(r_b)$ and $\nabla^2\rho(r_b)$ values (EML)

interaction	EPMM (kcal/mol)		EML (kcal/mol) (E_{HB})
	electrostatic term	total	
carboxylic O–H···O dimer			
(Exp)	-48.27	-47.48	-33.16
6-31G**	-44.11	-43.32	-33.09
TZVP	-36.71	-35.92	-32.99
trifurcated C–H···O dimer			
(Exp)	-12.45	-15.87	-3.15
6-31G**	-5.68	-9.09	-3.59
TZVP	-6.14	-9.55	-3.53
phenolic O–H···O dimer			
(Exp)	-9.54	-10.77	-4.38
6-31G**	-7.01	-8.24	-4.72
TZVP	-6.27	-7.50	-4.73
single C–H···O dimer			
(Exp)	-0.6	-1.82	-1.52
6-31G**	0.86	-0.36	-1.53
TZVP	-0.12	-1.34	-1.51

relationship between the derived terms such as kinetic energy density (G_{cp}), potential energy $V(r)$ density and the hydrogen bond energy (E_{HB}) are expressed in the following equations:⁷⁶

$$G_{\text{cp}} = \frac{3}{10}(3\pi)^{2/3}\rho_{\text{cp}}^{5/3} + \frac{\nabla^2\rho_{\text{cp}}}{6}$$

$$V(r) = \frac{1}{4}\nabla^2\rho(r) - 2G(r)$$

$$E_{\text{HB}} = \frac{1}{2}V_{\text{CP}}$$

The values of interaction energy obtained from the experimental and theoretical (6-31G** and TZVP) models are given in Table 5. The hydrogen bond energy values (E_{HB}) follow an order different from that of the dimers, as E_{HB} (O–H···O) is slightly more than the E_{HB} (trifurcated C–H···O).

Though this order seems to be contradicting the trend observed in dimeric interaction energies (Figure 9a,b), it is to be noted that while EPMM-calculated energies are dependent on the intermolecular geometry and the overall multipole populations, EML-energies focus on the local nature of the specific interactions in terms of $\rho(r_b)$ and $\nabla^2\rho(r_b)$ values.⁷⁷ Nevertheless, the small differences observed in interaction energy values suggest that the trifurcated C–H···O motif is in fact qualified to be comparable with the O–H···O hydrogen bond.

CONCLUSIONS

The topological properties derived from the experimental and theoretical charge density analysis on ferulic acid provide insights into the electrostatic nature of multifurcated weak hydrogen bonds. The quantitative properties derived from the charge density methods have been analyzed to describe the significance of lone pair directionality associated with the acceptor oxygen atom in the topology of trifurcated hydrogen bonds. The contribution of electrostatic component is evident in the interaction energies calculated by the EPMM method and in the electrostatic potential surfaces. In addition, interaction energies obtained from both experiment and theory validate, quantitatively, that a group of weak interactions can conjointly match or even surpass the strength of a strong classical hydrogen bond.

ASSOCIATED CONTENT

S Supporting Information

Crystallographic information file (CIF); F_{obs} vs F_{calc} scatter plot (Figures S1 and S2), fractal dimension plots (Figures S3–S5), distribution of reflections in equal-volume resolution shells (Table S1), details of CSD analysis (Table S2), and tables of topological features of covalent bonds (Tables S4–S6). This material is available free of charge via the Internet at <http://pubs.acs.org>.

AUTHOR INFORMATION

Corresponding Author

*E-mail: ssctng@sscu.iisc.ernet.in. Tel: +91-80-22932796. Fax: +91-80-23601310.

Notes

The authors declare no competing financial interest.

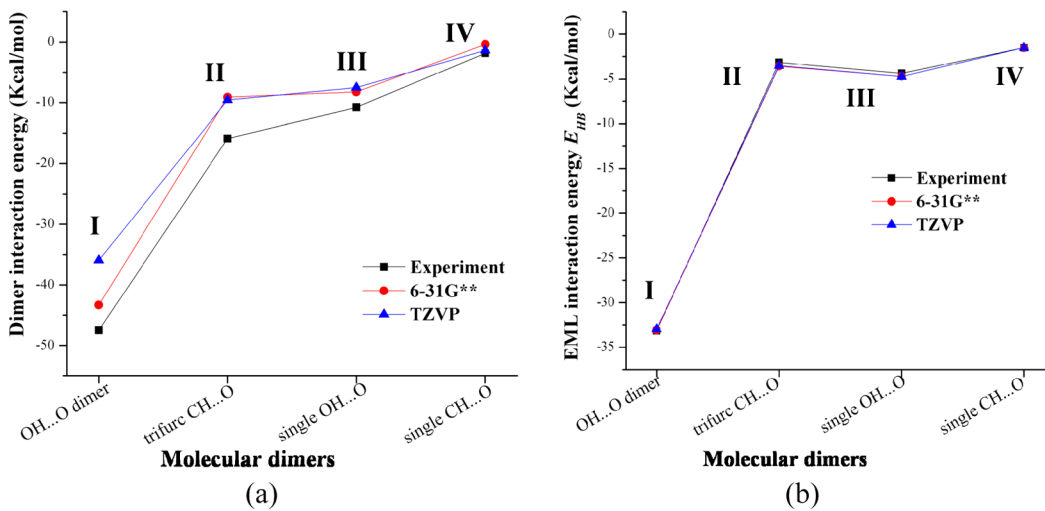


Figure 9. The trends in interaction energies of various molecular dimers estimated using (a) EPMM method, and (b) EML method.

ACKNOWLEDGMENTS

S.P.T. thanks UGC, India and MSP thanks Indian Institute of Science, Bangalore for the award of Senior Research Fellowships. T.N.G. thanks DST, India for the award of JC Bose fellowship.

REFERENCES

- (1) Desiraju, G. R.; Vittal, J. J.; Ramanan, A. *Crystal Engineering: A Textbook*; World Scientific Publishing Company Incorporated: Singapore, 2012.
- (2) Desiraju, G.; Steiner, T. Oxford University Press: Oxford, 1999; Vol. 9, p 507.
- (3) Espinosa, E.; Molins, E.; Lecomte, C. *Chem. Phys. Lett.* **1998**, *285*, 170–173.
- (4) Espinosa, E.; Souhassou, M.; Lachekar, H.; Lecomte, C. *Acta Crystallogr., Sect. B: Struct. Sci.* **1999**, *55*, S63–S72.
- (5) Espinosa, E.; Lecomte, C.; Molins, E. *Chem. Phys. Lett.* **1999**, *300*, 745–748.
- (6) Espinosa, E.; Molins, E. *J. Chem. Phys.* **2000**, *113*, 5686–5694.
- (7) Espinosa, E.; Alkorta, I.; Rozas, I.; Elguero, J.; Molins, E. *Chem. Phys. Lett.* **2001**, *336*, 457–461.
- (8) Espinosa, E.; Alkorta, I.; Elguero, J.; Molins, E. *J. Chem. Phys.* **2002**, *117*, 5529–5542.
- (9) Mallinson, P. R.; Smith, G. T.; Wilson, C. C.; Grech, E.; Woźniak, K. *J. Am. Chem. Soc.* **2003**, *125*, 4259–4270.
- (10) Dominiak, P. M.; Makal, A.; Mallinson, P. R.; Trzcińska, K.; Eilmes, J.; Grech, E.; Chruszcz, M.; Minor, W.; Woźniak, K. *Chem.—Eur. J.* **2006**, *12*, 1941–1949.
- (11) Desiraju, G. R. *Angew. Chem. Int. Ed. Eng.* **1995**, *34*, 2311–2327.
- (12) Desiraju, G. R. *Angew. Chem., Int. Ed.* **2007**, *46*, 8342–8356.
- (13) Dunitz, J. D.; Gavezzotti, A. *Angew. Chem., Int. Ed.* **2005**, *44*, 1766–1787.
- (14) Jeffrey, G. A.; Saenger, W. *Hydrogen Bonding in Biological Structures*; Springer-Verlag: Berlin, 1994.
- (15) Leonard, G. A.; McAuley-Hecht, K.; Brown, T.; Hunter, W. N. *Acta Crystallogr. Sect. D* **1995**, *51*, 136–139.
- (16) Mandel-Gutfreund, Y.; Margalit, H.; Jernigan, R. L.; Zhurkin, V. *B. J. Mol. Biol.* **1998**, *277*, 1129–1140.
- (17) Steiner, T.; Saenger, W. *J. Am. Chem. Soc.* **1993**, *115*, 4540–4547.
- (18) Derewenda, Z. S.; Derewenda, U.; Kobos, P. M. *J. Mol. Biol.* **1994**, *241*, 83–93.
- (19) Paton, R. S.; Goodman, J. M. *Org. Lett.* **2006**, *8*, 4299–4302.
- (20) Corey, E. J.; Rohde, J. J.; Fischer, A.; Azimioara, M. D. *Tetrahedron Lett.* **1997**, *38*, 33–36.
- (21) Jones, C. R.; Baruah, P. K.; Thompson, A. L.; Scheiner, S.; Smith, M. D. *J. Am. Chem. Soc.* **2012**, *134*, 12064–12071.
- (22) Desiraju, G. R. *Acc. Chem. Res.* **1991**, *24*, 290–296.
- (23) Steiner, T. *Angew. Chem., Int. Ed.* **2002**, *41*, 48–76.
- (24) Steiner, T. *Chem. Commun.* **1997**, 727–734.
- (25) Jeffrey, G. A. *An Introduction to Hydrogen Bonding*; Oxford University Press: New York, 1997; Vol. 12.
- (26) Nagawa, Y.; Yamagaki, T.; Nakanishi, H.; Nakagawa, M.; Tezuka, T. *Tetrahedron Lett.* **1998**, *39*, 1393–1396.
- (27) Qian, W.; Krimm, S. *J. Phys. Chem. A* **2002**, *106*, 6628–6636.
- (28) Koritsanszky, T. S.; Coppens, P. *Chem. Rev.* **2001**, *101*, 1583–1628.
- (29) Abramov, Y. A.; Volkov, A.; Wu, G.; Coppens, P. *Acta Crystallogr., Sect. A: Found. Crystallogr.* **2000**, *56*, 585–591.
- (30) Sosa, G. L.; Peruchena, N.; Contreras, R. H.; Castro, E. A. J. *Mol. Struct.: THEOCHEM* **1997**, *401*, 77–85.
- (31) Lo Presti, L.; Soave, R.; Destro, R. *J. Phys. Chem. B* **2006**, *110*, 6405–6414.
- (32) Woźniak, K.; Mallinson, P. R.; Wilson, C. C.; Hovestreydt, E.; Grech, E. *J. Phys. Chem. A* **2002**, *106*, 6897–6903.
- (33) Castellano, R. K. *Curr. Org. Chem.* **2004**, *8*, 845–865.
- (34) Yang, H.; Craven, B. *Acta Crystallogr. Sect. B: Struct. Sci.* **1998**, *54*, 912–920.
- (35) Mallinson, P. R.; Woźniak, K.; Smith, C. T.; McCormack, K. L. *J. Am. Chem. Soc.* **1997**, *119*, 11502–11509.
- (36) Munshi, P.; Venugopala, K. N.; Jayashree, B. S.; Guru Row, T. N. *Cryst. Growth Des.* **2004**, *4*, 1105–1107.
- (37) Munshi, P.; Guru Row, T. N. *Acta Crystallogr., Sect. B: Struct. Sci.* **2006**, *62*, 612–626.
- (38) Kubicki, M.; Borowiak, T.; Dutkiewicz, G.; Souhassou, M.; Jelsch, C.; Lecomte, C. *J. Phys. Chem. B* **2002**, *106*, 3706–3714.
- (39) Gatti, C.; May, E.; Destro, R.; Cargnoni, F. *J. Phys. Chem. A* **2002**, *106*, 2707–2720.
- (40) Desiraju, G. R.; Kashino, S.; Coombs, M. M.; Glusker, J. P. *Acta Crystallogr., Sect. B: Struct. Sci.* **1993**, *49*, 880–892.
- (41) Manoj, K.; Gonnade, R. G.; Shashidhar, M. S.; Bhadbhade, M. M. *CrystEngComm* **2012**, *14*, 1716–1722.
- (42) Bader, R. F. W. *Atoms in Molecules: A Quantum Theory*; Oxford University Press: Oxford, U.K., 1994.
- (43) Koch, U.; Popelier, P. L. A. *J. Phys. Chem.* **1995**, *99*, 9747–9754.
- (44) Vargas, R.; Garza, J.; Dixon, D. A.; Hay, B. P. *J. Am. Chem. Soc.* **2000**, *122*, 4750–4755.
- (45) Munshi, P.; Guru Row, T. N. *J. Phys. Chem. A* **2004**, *109*, 659–672.
- (46) Scheiner, S.; Kar, T.; Gu, Y. *J. Biol. Chem.* **2001**, *276*, 9832–9837.

- (47) Park, H.; Yoon, J.; Seok, C. *J. Phys. Chem. B* **2007**, *112*, 1041–1048.
- (48) Desiraju, G. R. *Acc. Chem. Res.* **1996**, *29*, 441–449.
- (49) Pacheco-Palencia, L. A.; Mertens-Talcott, S.; Talcott, S. T. *J. Agric. Food. Chem.* **2008**, *56*, 4631–4636.
- (50) Valentão, P.; Fernandes, E.; Carvalho, F.; Andrade, P. B.; Seabra, R. M.; Bastos, M. L. *J. Agric. Food. Chem.* **2001**, *49*, 3476–3479.
- (51) *Agilent Technologies*; 171.35.21 ed.; Agilent Technologies Ltd.: Yarnton, Oxfordshire, England, 2011.
- (52) Blessing, R. *J. Appl. Crystallogr.* **1997**, *30*, 421–426.
- (53) Sheldrick, G. *Acta Crystallogr., Sect. A: Found. Crystallogr.* **2008**, *64*, 112–122.
- (54) Farrugia, L. *J. Appl. Crystallogr.* **2012**, *45*, 849–854.
- (55) Hansen, N. K.; Coppens, P. *Acta Crystallogr., Sect. A: Found. Crystallogr.* **1978**, *34*, 909–921.
- (56) Volkov, A.; Macchi, P.; Farrugia, L. J.; Gatti, C.; Mallinson, P. R.; Richter, T.; Koritsanszky, T. S.; Version 5.34; University at Buffalo, State University of New York: New York, 2006.
- (57) Su, Z.; Coppens, P. *Acta Crystallogr., Sect. A: Found. Crystallogr.* **1998**, *54*, 357.
- (58) Hoser, A. A.; Dominiak, P. M.; Wozniak, K. *Acta Crystallogr., Sect. A: Found. Crystallogr.* **2009**, *65*, 300–311.
- (59) Allen, F. H.; Bruno, I. J. *Acta Crystallogr., Sect. B: Struct. Sci.* **2010**, *66*, 380–386.
- (60) Madsen, A. *J. Appl. Crystallogr.* **2006**, *39*, 757–758.
- (61) Munshi, P.; Madsen, A. O.; Spackman, M. A.; Larsen, S.; Destro, R. *Acta Crystallogr., Sect. A: Found. Crystallogr.* **2008**, *64*, 465–475.
- (62) Volkov, A.; Gatti, C.; Abramov, Y.; Coppens, P. *Acta Crystallogr., Sect. A: Found. Crystallogr.* **2000**, *56*, 252–258.
- (63) Lee, C.; Yang, W.; Parr, R. G. *Phys. Rev. B* **1988**, *37*, 785–789.
- (64) Becke, A. D. *J. Chem. Phys.* **1993**, *98*, 5648–5652.
- (65) Schafer, A.; Horn, H.; Ahlrichs, R. *J. Chem. Phys.* **1992**, *97*, 2571–2577.
- (66) Peintinger, M. F.; Oliveira, D. V.; Bredow, T. *J. Comput. Chem.* **2012**, DOI: 10.1002/jcc.23153.
- (67) Dovesi, R.; Saunders, V. R.; Roetti, C.; Orlando, R.; Zicovich-Wilson, C. M.; Pascale, F.; Civalleri, B.; Doll, K.; Harrison, N. M.; Bush, I. J.; D'Arco, P.; Llunell, M.; University of Torino: Torino, 2009.
- (68) Nethaji, M.; Pattabhi, V.; Desiraju, G. R. *Acta Crystallogr., Sect. C: Cryst. Struct. Commun.* **1988**, *44*, 275–277.
- (69) Meindl, K.; Henn, J. *Acta Crystallogr., Sect. A: Found. Crystallogr.* **2008**, *64*, 404–418.
- (70) Hirshfeld, F. *Acta Crystallogr., Sect. A: Found. Crystallogr.* **1976**, *32*, 239–244.
- (71) Spackman, M. A.; Munshi, P.; Dittrich, B. *ChemPhysChem* **2007**, *8*, 2051–2063.
- (72) Hübschle, C. B.; Dittrich, B. *J. Appl. Crystallogr.* **2011**, *44*, 238–240.
- (73) Volkov, A.; Koritsanszky, T.; Coppens, P. *Chem. Phys. Lett.* **2004**, *391*, 170–175.
- (74) Williams, D. E.; Cox, S. R. *Acta Crystallogr., Sect. B: Struct. Sci.* **1984**, *40*, 404–417.
- (75) Prins, L. J.; Reinhoudt, D. N.; Timmerman, P. *Angew. Chem., Int. Ed.* **2001**, *40*, 2382–2426.
- (76) Abramov, Y. *Acta Crystallogr., Sect. A: Found. Crystallogr.* **1997**, *S3*, 264–272.
- (77) Coppens, P.; Abramov, Y.; Carducci, M.; Korjov, B.; Novozhilova, I.; Alhambra, C.; Pressprich, M. R. *J. Am. Chem. Soc.* **1999**, *121*, 2585–2593.